LA-UR- 00-0091

Title: REVIEW AND ASSESSMENT OF MODEL UPDATING FOR NON-LINEAR, TRANSIENT DYNAMICS (U)

Author(s): François M. Hemez, Los Alamos National Laboratory, ESA-WR

Scott W. Doebling, Los Alamos National Laboratory, ESA-WR

Submitted to: Mechanical Systems and Signal Processing,
Vol. 15, No. 1, January 2001, pp. 45-74

Publication for the Special Issue of the Journal of Mechanical Systems and Signal Processing
"EuroMech-401, Inverse Methods in Structural Dynamics," Edited by J. E. Mottershead
Vol. 15, No. 1, January 2001, pp. 45-74.

REVIEW AND ASSESSMENT OF MODEL UPDATING FOR NONLINEAR, TRANSIENT DYNAMICS[1]

François M. Hemez[2] and **Scott W. Doebling**[3]
Engineering Analysis Group (ESA-EA)
Los Alamos National Laboratory, P.O. Box 1663, M/S P946
Los Alamos, New Mexico 87545, U.S.A.

ABSTRACT

The purpose of this publication is to motivate the need of validating numerical models based on time-domain data for nonlinear, transient, structural dynamics and to discuss some of the challenges faced by this technology. Our approach is two-fold. First, several numerical and experimental testbeds are presented that span a wide variety of applications (from nonlinear vibrations to shock response) and difficulty (from a single-degree of freedom system with localized nonlinearity to a 3D, multiple-component assembly featuring nonlinear material response and contact mechanics). These testbeds have been developed at Los Alamos National Laboratory in support of the advanced strategic computing initiative and our code validation and verification program. Conventional, modal-based updating techniques are shown to produce erroneous models although the discrepancy between test and analysis modal responses can be bridged. This conclusion offers a clear justification that metrics based on modal parameters are not well suited to the resolution of inverse, nonlinear problems. In the second part of this work, the state-of-the-art in the area of model updating for nonlinear, transient dynamics is reviewed. The techniques identified as the most promising are assessed using data from our numerical or experimental testbeds. Several difficulties of formulating and solving inverse problems for nonlinear structural dynamics are identified. Among them, we cite the formulation of adequate metrics based on time series and the need to propagate variability throughout the optimization of the model's parameters. Another important issue is the necessity to satisfy continuity of the response when several finite element optimizations are successively carried out. An illustration of how this problem can be resolved based on the theory of optimal control is provided using numerical data from a nonlinear Duffing oscillator. The publication concludes with a brief description of current research directions in inverse problem solving for structural dynamics.

---

[1] Authorized for unlimited, public release on January 14, 2000. LA-UR-00-0091. **This publication is unclassified.**

[2] Technical Staff Member, ESA-EA, hemez@lanl.gov, 505-665-7955 (Voice), 505-665-2137 (Fax).

[3] Technical Staff Member, ESA-EA, doebling@lanl.gov, 505-667-6950 (Voice), 505-665-2137 (Fax).

NOMENCLATURE

The “Standard Notation for Modal Testing & Analysis” is used throughout this paper, see Reference [1]. Symbols not commonly used in the modal testing and structural dynamics communities are defined in the text.

1. INTRODUCTION

Inverse problem solving is at the core of engineering practices as such work generally involves designing a system to target a given performance or to satisfy operating constraints. Increasingly, designers are faced with shorter design cycles while their testing capabilities are reduced and the physics they must understand becomes more sophisticated. The consequence is the need for larger-size computer models, coupled-field calculations and more accurate representations of the physics. To improve the predictive quality of numerical models and enhance the capability to extrapolate the response of a system, it is often necessary to formulate and solve inverse problems where simulations are compared to field measurements [2]. In addition, it has been recognized that non-deterministic approaches must be employed to alleviate our lack of test data and incomplete understanding of mechanics [3].

The work presented in this publication deals with the formulation of inverse problems for correlating transient dynamics to responses obtained from nonlinear finite element models. The application targeted is clearly structural dynamics although most of the techniques discussed here either originate or find their counterparts in physics and other engineering fields. The reason why time series rather than modal parameters are considered is essentially because the increasing complexity and sophistication of engineering applications makes it necessary to analyze systems with arbitrary sources of uncertainty and nonlinearity. Another motivation is the modeling of highly transient dynamic events for which modal solutions make no sense due to the clustering of high-frequency modes and because modal damping can not capture with a sufficient degree of accuracy the energy dissipation mechanism involved.

For clarity, this paper is organized according to three main parts. First, a brief discussion of current trends in testing, modeling and computing for structural dynamics applications is provided (Section 2). The purpose of this discussion is to provide insight regarding the issues that, to our opinion, inverse problem solving will have to address in the near future. Then, several numerical and experimental testbeds are presented (Section 3). These are used for generating reference data or test data that feed various test-analysis reconciliation techniques. Our intent is to introduce a series of problems that feature various sources of nonlinearity and modeling difficulties and that challenge the existing model updating strategies. The second part of this publication reviews the state-of-the-art in model updating and error control algorithms for nonlinear dynamics (Sections 4 and 5). Several techniques are illustrated using our numerical or experimental testbeds. This demonstration is not intended as a thorough comparison between different model updating algorithms nor as an exhaustive assessment of each method’s

advantages and limitations. The objective is rather to identify the critical deficiencies of the technology currently available with the ultimate goal of developing tools for assessing the predictive quality of a stochastic, nonlinear numerical model. Finally, the third part of this publication presents some of the key aspects that, we believe, will drive the development of test-analysis correlation and model validation technology in the years to come (Section 6).

2. CURRENT CHALLENGES IN INVERSE PROBLEM SOLVING

In this Section, some of the current trends in testing, modeling and computing for structural dynamics applications are briefly discussed. Our purpose is to introduce the challenges faced by inverse problem solving and to motivate the particular choice of the testbeds presented in Section 3.

2.1. TRENDS IN STRUCTURAL DYNAMICS

The main reason why numerical models have become so popular is because it is much less expensive to use computational time than it is to run a sophisticated experiment. Many practical situations also occur where the phenomenon of interest can not be measured directly. Hence, the scientific community has turned to numerical models that can be parametrized and used to study a wide variety of situations. This argument has been reinforced in recent years by the increasing efficiency of processors, the greater availability of memory, the breakthrough of object-oriented data structures together with the growing popularity of parallel processing whether it involves computers with massively parallel architectures or networks of single-CPU workstations. Interestingly enough, the miniaturisation of CPU's and their greater efficiency have influenced greatly testing procedures, making it possible to instrument structures with hundreds of transducers. Powerful data analysis and friendly computer graphics are also a driving force behind the development of non-intrusive, optical measurement systems such as holography and laser vibrometry. These technological breakthroughs are not without major consequences on the way engineers analyze structural systems and on their conception of test-analysis correlation and inverse problem solving.

An illustration of this evolution is the rapid development of modeling procedures for nonlinear dynamics. It is reasonable to foresee that the bottleneck of computing power will be removed in the near future, at least when it comes to engineering applications.[4] Consequently, research and development efforts in recent years have been mostly focused on improving the representation of the geometry and the physics. Examples are the derivation of small-scale, statistical models for contact dynamics; the implementation of high-fidelity, nonlinear material models; or the efforts to expand our current modeling capabilities to the high frequency range for predictive acoustics. In

[4] The Accelerated Strategic Computing Initiative (ASCI) platforms "BlueMountain" and "Red" at Los Alamos National Laboratory and Sandia National Laboratories routinely perform over 3 Teraflops distributed over several thousand computational nodes. This power may not yet enable high-energy physics simulations with enough accuracy but it is considered sufficient for most engineering applications. For reference, see: www.sgi.com/ newsroom/press_releases/2000/may/blue_mountain.html.

spite of these undeniable advances, very rarely have the issues of uncertainty quantification and predictability been raised. These are central questions when it comes to assessing whether a numerical simulation is capable of reproducing with acceptable accuracy the experiment it is supposed to replace. It is therefore reasonable to state that, no matter how powerful computers become, there will always be some degree of uncertainty in the numerical models due to unknown interfaces, unknown physics, environmental variability, parameter and assembly uncertainty, idealization errors, discretization errors, numerical errors, etc. Increased computational power allows to bound some of these sources of uncertainty (such as discretization and numerical errors), but not all of them can be reduced to desirable levels. Because the trend of replacing expensive laboratory or field experiments with numerical simulations is not going to change, systematic model validation and inverse problem solving strategies are needed that must be capable of handling large-size numerical models geared at capturing time-dependent, stochastic and nonlinear phenomena.

2.2. SPECULATIVE OUTLOOK

When analyzing the dynamic response of a complex system using the Finite Element (FE) method, it is not acceptable to neglect the contribution of an important component, joint or interface. In the past, neglected dynamics were accounted for by tuning parameters in the model to agree with the experimental data. For example, the damping (modal or other) was determined "ad hoc" using test data obtained from testing the fully assembled system. Then, the identified damping properties were added to the model to improve its predictive accuracy. At present, some of the full-scale testing capabilities which formerly existed at the U.S. national laboratories and many other facilities in the automotive, aerospace and civil engineering communities are no longer functional. Therefore, it is no longer possible to reconcile a model with experimental data for all environments. In the future, models will be constructed with limited use of these expensive, full-scale test data sets. In addition, it is our opinion that structural dynamics in the 21st century will become increasingly:

1) Nonlinear;
2) Non-structural;
3) Non-modal;
4) High bandwidth;
5) Multi-physics.

In these conditions, can the concept of FE model updating that has been developed for linear, modal dynamics be generalized? Is FE model updating the correct answer to model validation? What "features" other than the conventional mode shapes and resonant frequencies can be extracted from the data to characterize the response of a nonlinear system? How to quantify the total uncertainty of an experiment? How to propagate the parametric uncertainty of a numerical simulation? These are some of the long-term questions that, we believe, should be

addressed by the structural dynamics community at large in order to develop inverse problem solving techniques that would be relevant to tomorrow's structural dynamics applications.

3. TESTBEDS FOR THE VALIDATION OF NONLINEAR STRUCTURAL MODELS

In this Section, several numerical and experimental testbeds are presented. They have been found in the literature or developed in support of the advanced strategic computing initiative and our code validation and verification program. Aside from programmatic work, they are also used to answer some of the questions mentioned in previous Section 2. The examples discussed span a wide variety of applications and difficulty. The first three involve nonlinear vibrating systems (Sections 3.1.1, 3.1.2 and 3.2). The fourth one represents a high-frequency, transient shock response (Section 3.3). The fifth one represents the response of a full, assembled system to an explosive load (Section 3.4). The sources of nonlinearity considered are either purely analytical (cubic springs), undetermined but localized (impact mechanism) or parametric and distributed (hyper-foam material and contact dynamics). These examples also feature various mechanisms for the dissipation of energy that can not, we believe, be reduced to the conventional, modal representation of damping.

3.1. NUMERICAL TESTBEDS WITH A CUBIC NONLINEARITY

The first two examples are purely analytical. They represent point masses and linear springs. Damping is considered in the first case only. The first system exhibits a single degree of freedom and the second system has four degrees of freedom. In both cases, the source of nonlinearity considered is a cubic spring, that is, the nonlinear, internal force is proportional to the third power of a displacement. Advantages of these numerical simulators is that the modeling error, the nonlinear perturbation introduced and the noise-to-signal ratio can be controlled explicitly.

3.1.1. *Single Degree of Freedom Oscillator*

Our first numerical testbed is the single degree of freedom system pictured in Figure 1. This system is also known as the Duffing oscillator and it has been studied extensively for the ability of its response $x(t)$ to transition from ordered to chaotic behavior. The equation of motion, the harmonic forcing function considered here and the nonlinear, internal force are defined in equation (1). In the numerical tests performed, reference data are generated by integrating equation (1) over a period of 30 seconds. Then, the internal force is assumed to be unknown which introduces a modeling error. The purpose of test-analysis correlation and FE model updating would typically be to identify this missing term as a function of time.

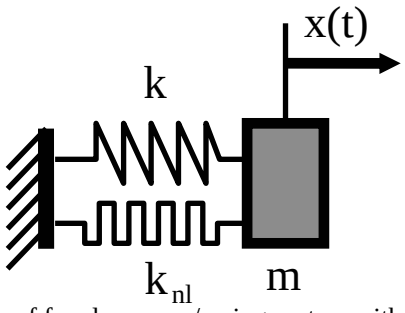

Figure 1. Single degree of freedom mass/spring system with a cubic nonlinearity.

$$m\frac{\partial^2 x}{\partial t^2}(t) + d\frac{\partial x}{\partial t}(t) + kx(t) + F_{int}(t) = F_{ext}(t)$$
$$F_{ext}(t) = F_o \cos(\Omega t); F_{int}(t) = k_{nl} x^3(t) \tag{1}$$
$$m = 2.56; d = 0.32; k = 1; k_{nl} = 0.05; F_o = 2.5; \Omega = 1$$

In the example discussed in Section 5, simulated "measurements" are assumed to be available only at 11 or 151 equally-spaced samples. They consist of displacement and velocity data. Although this testbed is probably the simplest one that could be imagined, the amount of computation required for solving the inverse problem may be enormous (see Section 5). Figure 2 shows the difference between test and analysis time-histories before the model is optimized. Displacements are shown on the top half and velocities are shown on the bottom half. Clearly, the response predicted by the linear model is inconsistent with test data.

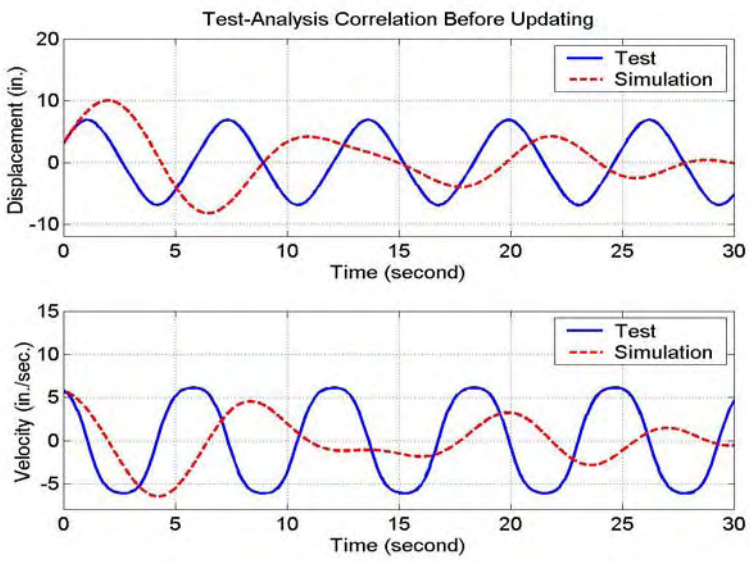

Figure 2. Test-analysis correlation of the single degree of freedom system before model updating.
(Top half, displacement time-history; Bottom half, velocity time-history.)

3.1.2. *Multiple-Degree of Freedom Oscillator*

The second system investigated is a 4-degree of freedom, mass/spring system with cubic nonlinearity. Figure 3 provides an illustration and the nonlinear, internal force added to the equation of motion is defined in equation (2). This system generalizes the Duffing oscillator to a multiple-degree of freedom case. A higher dimensionality is required to study the effect of spatial incompleteness, that is, the effect of measuring the response at a subset of the model's degrees of freedom. The system shown in Figure 3 is numerically excited with a random excitation and implicit time integration is used for obtaining the acceleration response at the four degrees of freedom.

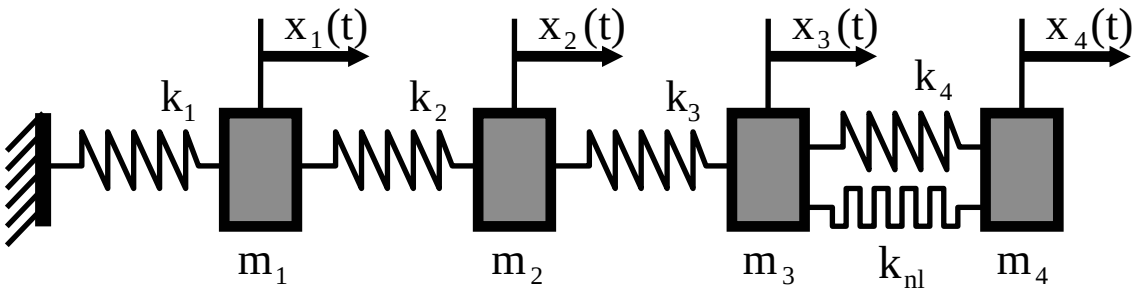

Figure 3. 4-degree of freedom mass/spring system with a cubic nonlinearity.

$$\{\mathbf{F}_{\mathbf{int}}(\mathbf{t})\} = \begin{Bmatrix} \mathbf{0} \\ \mathbf{0} \\ \mathbf{0} \\ \mathbf{k}_{\mathbf{nl}}\left(\mathbf{x}_4(\mathbf{t}) - \mathbf{x}_3(\mathbf{t})\right)^3 \end{Bmatrix} \tag{2}$$

Although these results are not presented here, we performed several numerical experiments where the objective was to recover a 15% stiffness reduction of the third linear spring when one of the system's output was unknown.[5] The overall performance of time-domain model updating was studied using various configurations where, among other things, 1) features used to characterize the data were varied; 2) the noise-to-signal ratio was varied; and 3) the nonlinear force was known or unknown. The performance of three FE model reduction techniques was also studied and whether or not model reduction could be combined to parametric model updating for nonlinear dynamics. The results obtained so far indicate that some of the model reduction techniques tested provide a valuable alternative to the conventional modal expansion even when the dynamics of interest are significantly nonlinear. The reader is referred to References [4] and [5] for further details about these investigations.

[5] Data provided to the FE model updating algorithms consisted of the acceleration "measurements" at locations 1, 3 and 4 only.

3.2. EXPERIMENTAL TESTBED FOR NONLINEAR VIBRATIONS

Our testbed for model validation in the context of nonlinear vibration is the LANL 8-DOF system (which stands for Los Alamos National Laboratory eight degrees of freedom system) illustrated in Figure 4. It is formed with eight translating masses connected by springs. Each mass is a disc of aluminum 25.4 mm thick and 76.2 mm in diameter with a center hole. The hole is lined with a Teflon bushing. There are small steel collars on each end of the discs. The masses all slide on a highly polished steel rod that supports the masses and constrains them to translate along the rod. The masses are fastened together with coil springs epoxied to the collars that are, in turn, bolted to the masses. The support rod introduces a source of friction that constitutes the first modeling challenge.

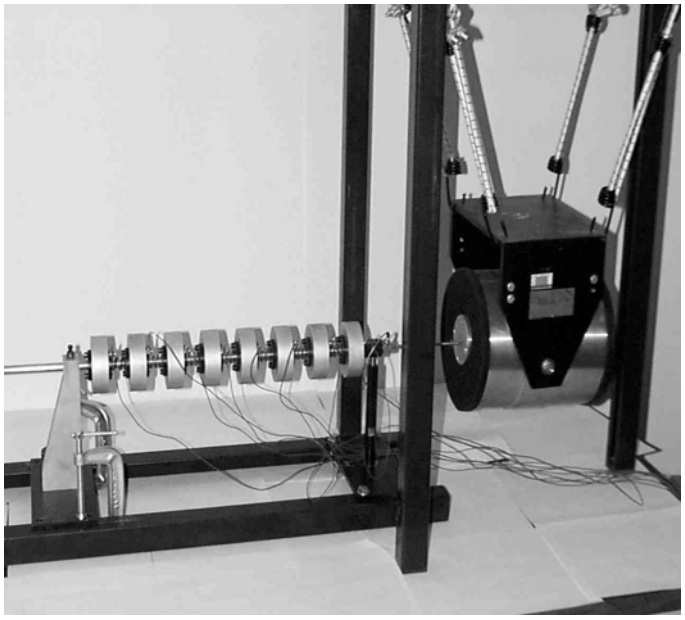

Figure 4. LANL 8-degree of freedom testbed. Illustration of the system and its support stand.

Vibration tests are performed on the nominal system and on a damaged version where the stiffness of one of the springs is reduced by 14%. The excitation applied at the driving point measurement consists of a random signal at various force amplitudes. The time-domain acceleration responses are collected at all eight masses over a period of eight seconds with a total of 2^{13} = 8,192 samples. Figure 5 illustrates the response obtained at the first and fifth sensors during one of the tests performed with the linear, undamaged configuration of the LANL 8-DOF system. The first step of this experiment is to identify the system's modal parameters using a classical frequency-domain curve fitting algorithm. Table 1 shows that the original, linear and undamped FE model is in good agreement with the identified modal parameters prior to any parametric adjustment. The more-or-less uniform shift in frequency seen in Table 1 for the first three modes is caused by the driving point attachment system whose mass was originally over-estimated in the FE representation. This error was subsequently corrected by performing a few iterations of modal-based, parametric adjustment. (The model updating technique employed for this purpose is the force-based

residual approach reviewed in Section 4.) This update reduces the frequency errors to 1% in average and brings the Modal Assurance Criterion (MAC) over 99% for the first five modes.

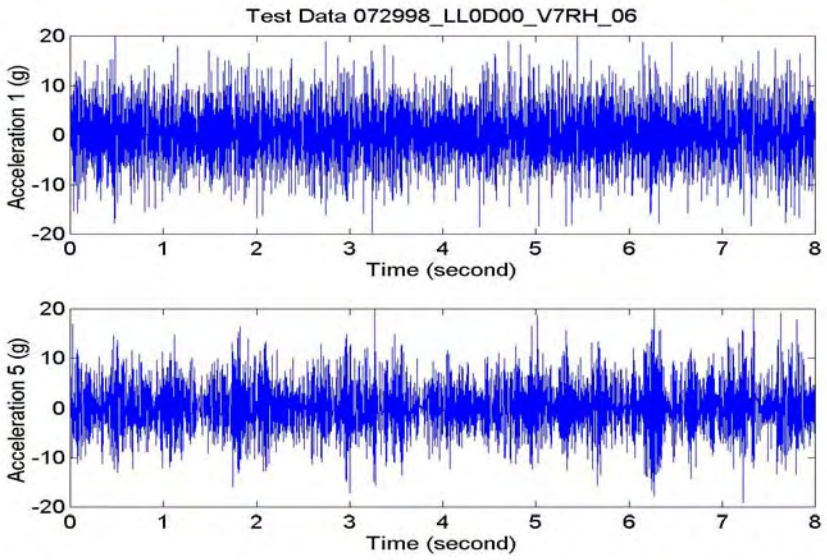

Figure 5. Typical acceleration response at sensors 1, 5. (Linear, undamaged LANL 8-DOF system.)

Table 1. Test-analysis correlation of the LANL 8-DOF testbed. (The table shows the correlation between the nominal, undamaged system and the corresponding linear model.)

Mode Number	Identified Frequency	Identified Damping Ratio	FE Model Frequency	Modal Assurance Criterion (MAC)	Frequency Error
1	22.6 Hz	8.5%	21.8 Hz	99.7%	-3.5%
2	44.5 Hz	4.3%	43.0 Hz	99.4%	-3.4%
3	65.9 Hz	3.3%	63.0 Hz	99.4%	-4.4%
4	86.6 Hz	5.0%	80.8 Hz	93.2%	-6.7%
5	99.4 Hz	2.6%	95.6 Hz	98.5%	-3.8%

A contact mechanism can also be added between two masses to induce a source of contact/impact. The hardware used for this purpose is pictured in Figure 6. A bumper is placed on one mass that limits the amount of motion that mass may move relative to the adjacent mass. When the distance between the ends of the rods is equal to the initial clearance, impact occurs. This impact simulates damage caused by spring deterioration to a degree which permits contact between adjacent masses, or in a simplified manner, the impact from the closing of a crack during vibration. The degree of damage is controlled by changing the amount of relative motion permitted before contact, and changing the hardness of the bumpers on the impactors. This testbed is designed to simulate situations where a mostly linear system is connected to a secondary component. A common example is the dynamics of a delivery vehicle-payload assembly. Nonlinearity and energy dissipation mechanisms are generally introduced at the

interface between the two by the attachment system. Although the dynamics of the whole system may remain mostly linear, accounting for the nonlinear perturbation introduced by the interface may be important for predictability purpose. Likewise with the LANL 8-DOF system, the sources of nonlinearity (friction, impact) have a sensible effect on the mostly linear dynamics. This is illustrated in Figures 7 and 8 that show how the resonant frequencies and modal damping ratios identified from the time-domain acceleration data vary as the impact mechanism is activated and the input force level is increased. As expected, these sources of nonlinearity do not modify significantly the distribution of mass and stiffness. As a result, the identified frequencies shown in Figure 7 are relatively insensitive to the impact and input force level. On the other hand, activating the bumping mechanism has the effect of promoting more energy dissipation which translates into higher damping (for a given mode) as shown in Figure 8. Increasing the input force level overall decreases damping because less "stick and slip" friction is obtained at higher forcing levels.

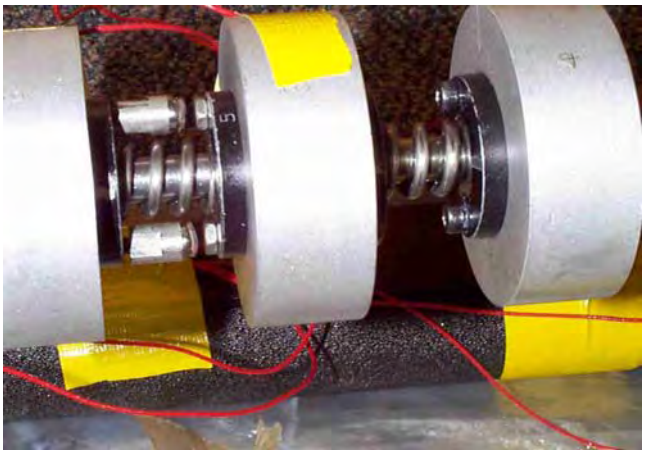

Figure 6. LANL 8-degree of freedom testbed. Contact mechanism between masses 5 and 6.

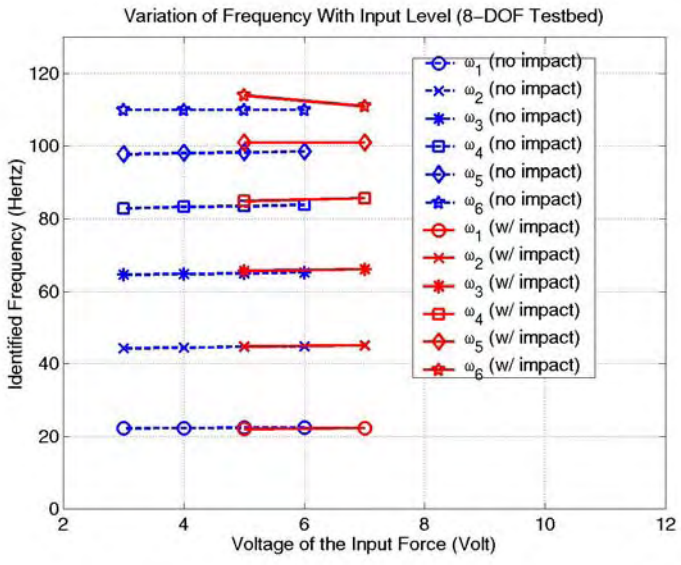

Figure 7. Effect of the nonlinearity (friction, impact) on the identified resonant frequencies.

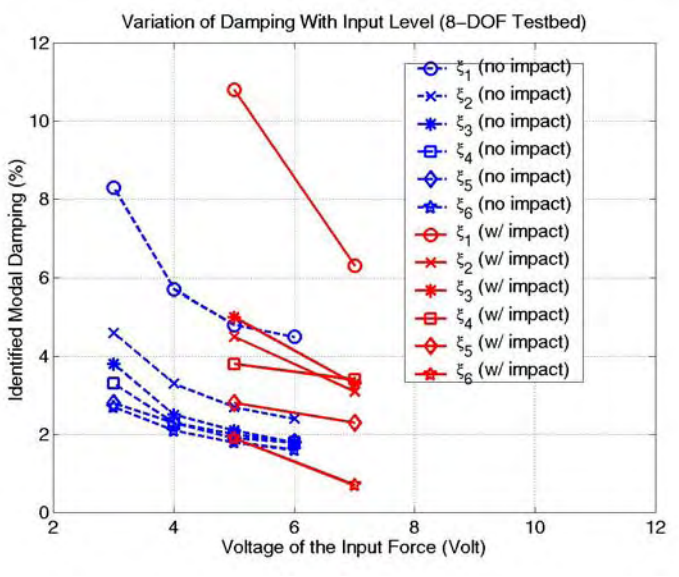

Figure 8. Effect of the nonlinearity (friction, impact) on the identified modal damping ratios.

The test discussed in this publication consists of identifying the damaged spring (14% stiffness reduction) using a linear model that does not account for the friction nor the source of contact/impact. The performance of conventional model updating approaches is evaluated when the distance between test data and modeling is defined using modal parameters (resonant frequencies and mode shapes). Time-domain techniques are also tested for their ability to identify the (unknown) nonlinearity when less measurements than degrees of freedom are available. Finally, we mention that test data from the 8-DOF LANL testbed can be made available to assess model validation strategies. We believe that this is an interesting testbed because small-dimension, linear models can be developed that provide a good starting point for test-analysis correlation. Nevertheless, some of the configurations tested allow to discriminate between numerical techniques that would perform well when the dynamics remains linear but that fail when nonlinear effects dominate the response.

3.3. IMPACT TEST EXPERIMENT

The next testbed presented deals with transient responses rather than nonlinear vibrations. The application targeted is a high-frequency shock experiment that features a component characterized by a nonlinear, visco-elastic material behavior. Results of several explicit FE simulations are compared to field measurements and parameters of the numerical models are optimized to improve the correlation.

An illustration of the setup is provided in Figure 9 and the actual hardware used during impact testing is pictured in Figure 10. The system tested is composed of two components (steel impactor, foam pad) assembled to

the carriage (impact table) in a rather straightforward manner. The center of the steel cylinder is hollow and has been fixed with a rigid collar to restrict the motion of the impactor to the vertical direction. This assures perfectly bilinear contact between the steel and foam components, allowing the structure to be modeled axi-symmetrically. In spite of this, a full three-dimensional model is developed to verify this assumption's validity. Besides the material modeling, another important parameter in this study is the amount of preload applied by the bolt used to hold the assembly together. The torque applied was not measured during testing. It is very likely to have varied from test to test which introduces a significant source of uncertainty in the numerical simulation.

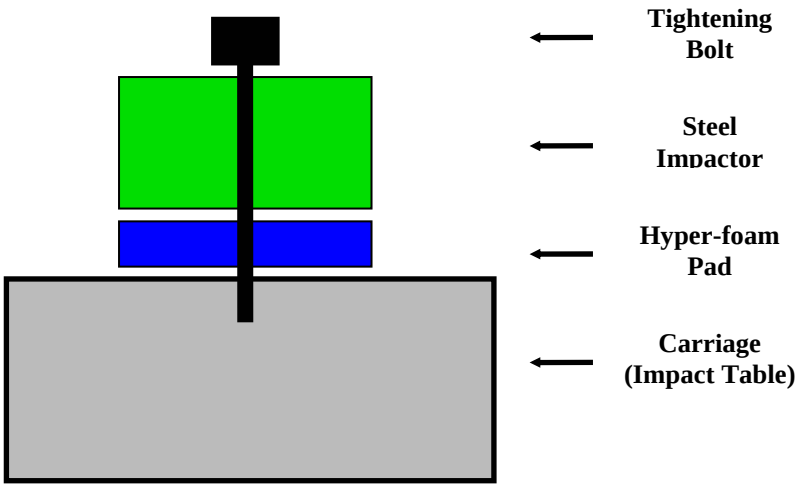

Figure 9. Description of the assembly of the cylindrical impactor and carriage.

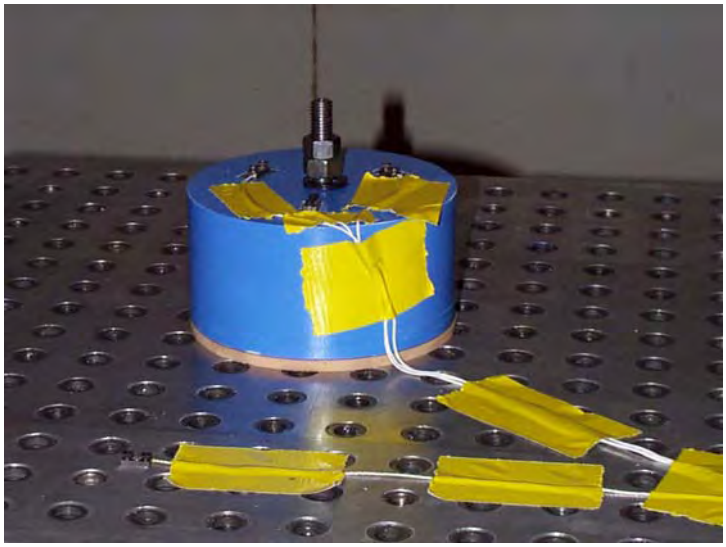

Figure 10. LANL impact test setup.

The analysis program used for these calculations is HKS/Abaqus-Explicit, a general-purpose package for finite element modeling of nonlinear structural dynamics [6]. It features an explicit time integration algorithm, which is convenient when dealing with nonlinear material behavior, potential sources of impact or contact, and high frequency excitations. In an effort to match the test data, several FE models are developed by varying, among other

things, the constitutive law and the type of modeling. Therefore, optimization variables consist of the usual design variables augmented with structural form parameters such as kinematic assumptions, geometry description (2D or 3D), contact modeling and numerical viscosity. Figure 11 illustrates one of the discretized models used for numerical simulations.

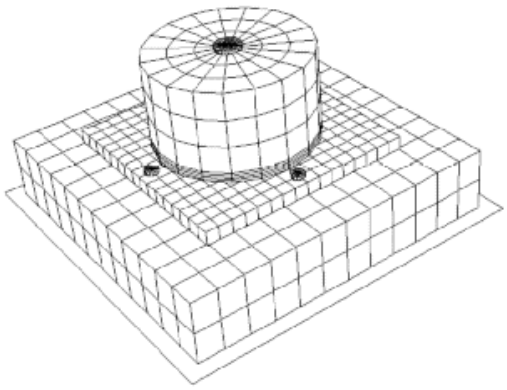

Figure 11. 3D model of the LANL impact testbed.

During the actual tests, the carriage that weights 955 lbm (433 kg) is dropped from various heights and impacts a rigid floor. The input acceleration is measured on the top surface of the carriage and three output accelerations are measured on top of the steel impactor that weights 24 lbm (11 kg). The location of the four sensors can be seen on Figure 10. Impact tests are repeated several times to collect multiple data sets from which the repeatability of the experiment can be assessed. Table 2 gives the number of data sets collected for each configuration tested. Dropping the carriage from two different heights results into different velocities at the time of impact. The values obtained by integrating the acceleration signal match the analytical formula $\dot{\mathbf{x}}_{\mathbf{impact}} = \sqrt{\mathbf{2gh}_{\mathbf{drop}}}$ and provide 60.4 in./sec. (1.5 m/sec.) and 222.9 in./sec. (5.7 m/sec.) for the low velocity and high velocity impacts, respectively. The reason why less data sets are available at high impact velocity is because these tests proved to be destructive to the elastomeric pad and could not be repeated to study the variability.

Table 2. Data collected with the impact testbed.

Number of Data Sets Collected	Low Velocity Impact (13 in./0.3 m Drop)	High Velocity Impact (155 in./4.0 m Drop)
Thin Layer (0.25 in./6.3 mm)	10 Tests	5 Tests
Thick Layer (0.50 in/12.6 mm)	10 Tests	5 Tests

Upon impact, the steel cylinder compresses the foam pad to cause elastic and plastic strains during a few μ-seconds. Typical accelerations measured during the impact tests are depicted in Figure 12. Both data sets are

generated by dropping the carriage from an initial height of 13 inches (0.33 meters). Figure 12 shows on top the acceleration response when a 1/4 inch-thick (6.3 mm) foam pad is used and it shows on the bottom the acceleration response with a 1/2 inch-thick (12.6 mm) foam pad. It can be seen that over a thousand g's are measured on top of the impact cylinder which yields large deformations in the foam pads. The time scale also indicates that the associated strain rates are important. Lastly, the variation in peak acceleration observed in Figure 12 suggests that non-zero angles of impact are involved, making it necessary to model this system with a 3D discretization. Clearly, modal superposition techniques would fail because of the following reasons: 1) contact can not be represented efficiently from linear mode shapes; 2) nonlinear hyper-foam models, that possibly include visco-elasticity, are needed to represent the foam's hardening behavior; and 3) very refined meshes would be required to capture the frequency content over 10,000 Hz. Although it may be possible to compute the solution via modal superposition for a single design, repeating this procedure in the context of inverse problem solving would be totally unfeasible.

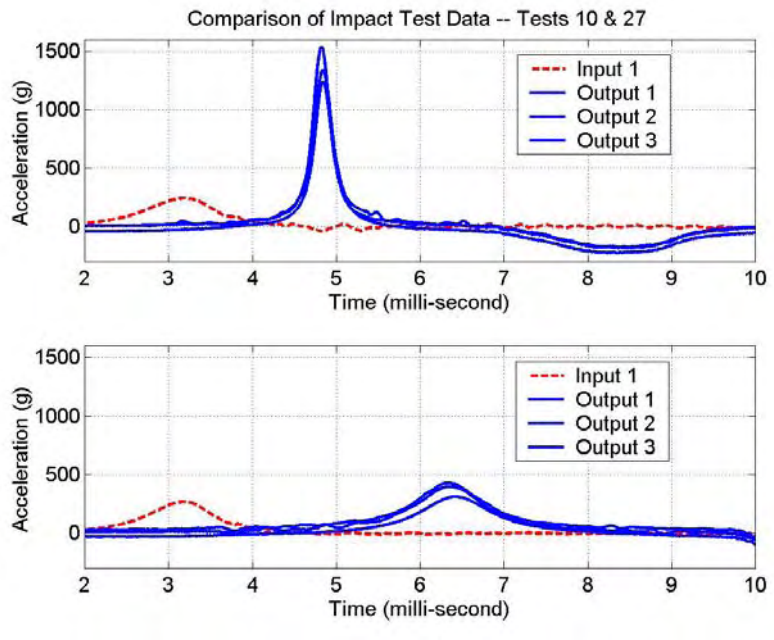

Figure 12. Input and output accelerations measured during a low-velocity impact.
(Top: low-velocity impact of a thin foam pad; Bottom: low-velocity impact on a thick foam pad.)

Since several data sets are available for the same configuration tested (see Table 2), the total uncertainty of the experiment can be estimated. Figure 13 illustrates the variability in peak acceleration obtained when the same test is repeated ten times (low impact, thin pad configuration). Although the environment of this particular experiment was controlled very thoroughly, Figure 13 shows that a significant spread in the acceleration response is obtained. This variability is believed to be caused essentially by random changes in the boundary condition, the angles of impact and the preload applied by the tightening bolt. The purpose of test-analysis correlation should therefore not be to reproduce a particular data set but rather to predict the distribution of experimental results at a given level of accuracy. The impact testbed also serves the purpose of assessing the performance of statistical sampling strategies

and fast probability integration algorithms used to propagate uncertainty through the forward analysis. Statistical analysis techniques used for this application rely on the orthogonal array sampling and the Latin Hyper-cube sampling presented in Reference [7]. Fast probability is provided via the software package NESSUS and interfaced to our explicit FE analysis and parallel processing capabilities [8].

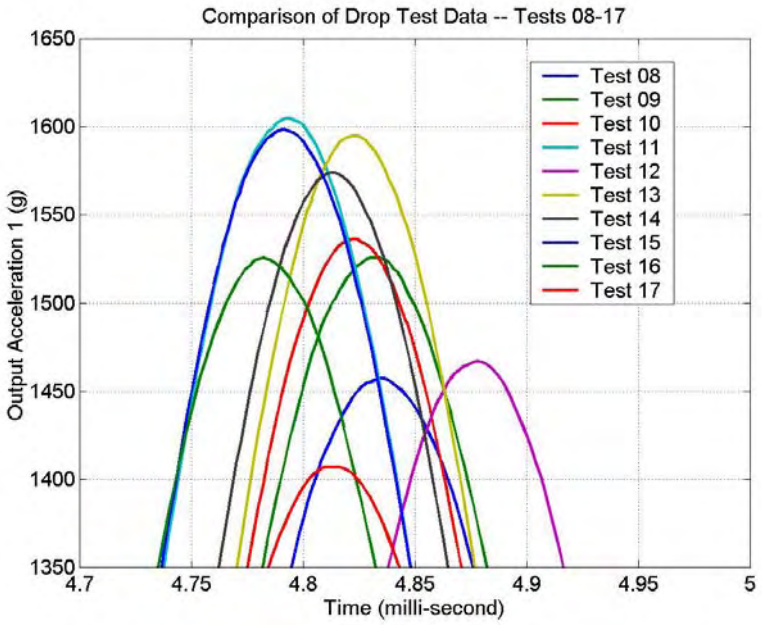

Figure 13. Variability of the acceleration response at output sensor 1.
(Impact test considered: 13 in./low-velocity impact of a 0.25 in./thin foam pad.)

3.4. FORWARD MOUNT IMPULSE TESTING

The last testbed discussed represents a fully integrated system as opposed to the phenomenological or component experiments presented in Sections 3.1 to 3.3. It involves a complex engineering application performed at Los Alamos National Laboratory for the Accelerated Strategic Computing Initiative (ASCI). The U.S. Department of Energy's ASCI program is aimed at developing massively parallel hardware and software environments for enhancing the modeling, predictive quality and reliability of computer simulations for high-energy physics and engineering applications.

The system tested is an assembly of sub-components (inside shell; outside shell; support structure; electronics package and payload simulators) that feature complex joints subjected to an impulse load. The impulse is generated by detonating an explosive grid on the surface of the structure as shown in Figure 14.

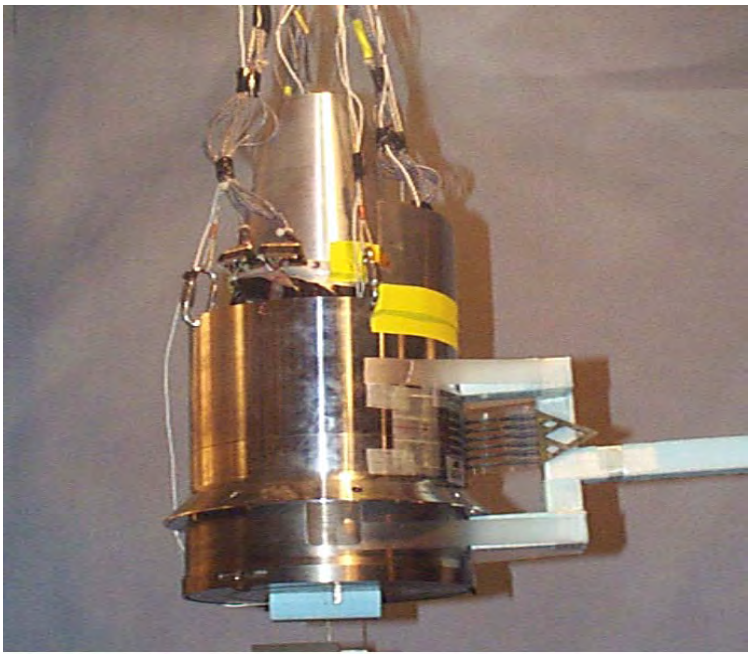

Figure 14. Instrumented test item with the explosive grid ready to detonate.

A total of 33 strain gauges and 6 accelerometers instrument the response of this system with sampling rates as high as 20 MHertz. Figure 15 shows typical strain and acceleration responses obtained during one of the tests performed. Figure 16 illustrates the shock response spectrum obtained from the 6th acceleration response. Shock response analyses allow designers to estimate, for example, the peak acceleration transmitted to an electronics component as a function of the component's fundamental resonant frequency. Figure 16 clearly shows that most of the system's dynamics is identified in the 5-30 KHertz range which would render the development of a high-accuracy modal model a prohibitively computationally expensive task.

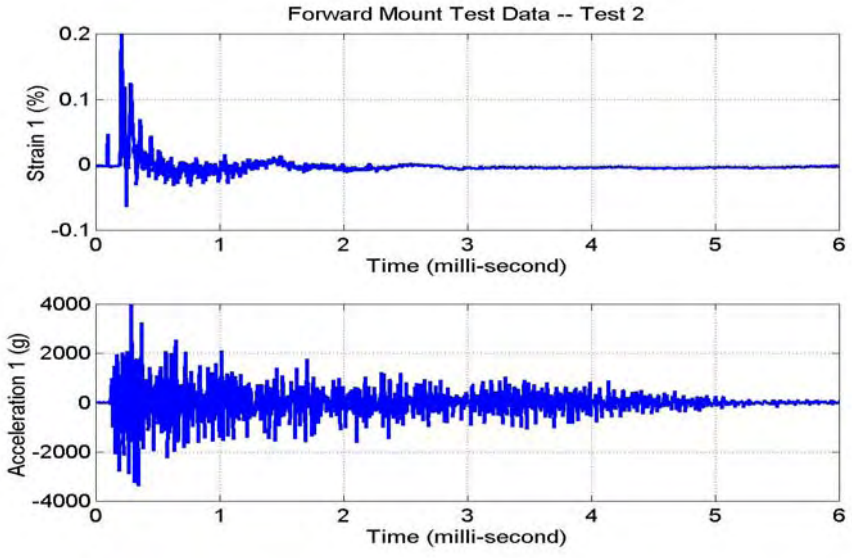

Figure 15. Measured strain and acceleration responses.
(Top: strain at sensor 1; Bottom: acceleration at sensor 1.)

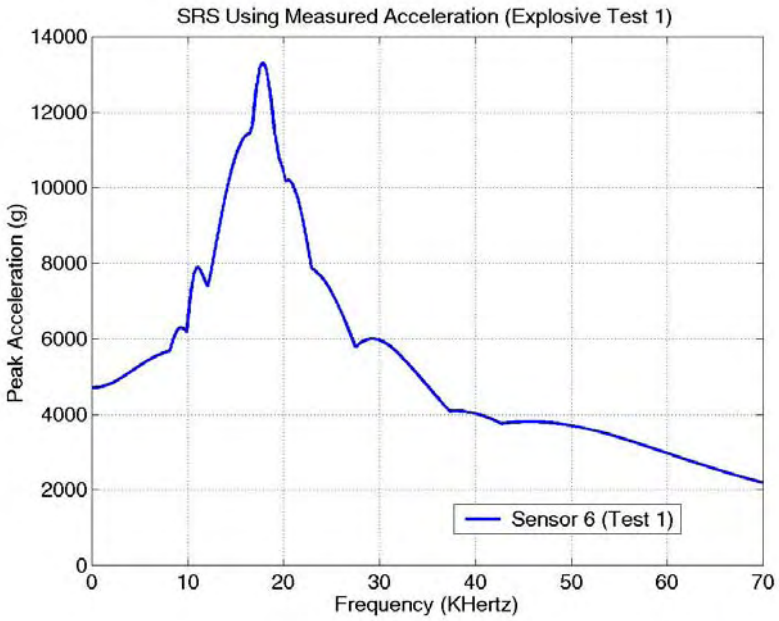

Figure 16. Shock response spectrum obtained from acceleration sensor 6.

A fully 3D model is developed that includes a very detailed representation of the geometry, material nonlinearities, and contact surfaces including pre-loading. Different materials are involved in this system (aluminum, stainless steel, carbon steel and titanium) which makes it more difficult to implement accurate models for the contact dynamics. The resulting nonlinear, explicit model features in the order of 1.4 million elements and 5 million degrees of freedom. It is analyzed on the ASCI platform "BlueMountain" with 504 dedicated processors. Typically, one hour of CPU time is required to simulate 10^{-3} second of response. As before, several tests are carried out to assess the degree of variability of the assembly. Figure 17 compares two strain measurements obtained at the same location when different torque values are applied to the assembly between the inside shell and the outside shell. Although the two curves offer many similarities in terms of peak response and frequency content, the initial time-delay indicates a variation in the contact mechanics of the main threaded joint. Therefore, modeling and analyzing this system in the time domain requires the analysts to address the stochastic nature of the experiment as well as the wave propagation, contact mechanics, pre-loading, interface modeling and nonlinear dynamics involved.

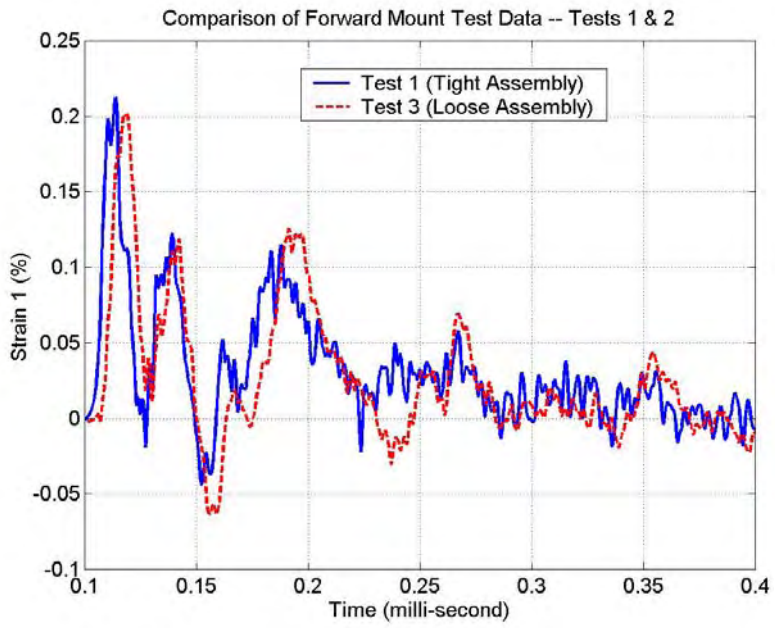

Figure 17. Comparison of strain time-histories measured at sensor 1.

The ultimate goals of the impulse experiment are to validate our modeling methods, identify specific joint behaviors and quantify the degree of variability of the assembly. Because of the computational cost involved, the ability to analyze this system relies strongly on the capability to propagate efficiently uncertainty and variability through the forward calculation. Again, statistical sampling and analysis methods are being evaluated to meet this first objective. Also, such large computer simulations tend to generate enormous amounts of output that must be synthesized into a small number of indicators for the analysis. This step is referred to as feature extraction [2] in the following. The main issue in feature extraction is to define indicators that provide meaningful insight regarding the ability of the model to capture the dynamics investigated. Several features are used for analyzing this nonlinear, transient data sets that include: conventional modal analysis; Fourier transforms; the principal component decomposition; the shock response spectrum; ARX and ARMA-based features; the power spectral density; higher-order statistical moments; and probability density functions.

Figure 18 illustrates a typical correlation obtained between the test data and the explicit FE simulation after a few critical parameters of the numerical model have been adjusted. The emphasis of this preliminary update was to match the peak strain at a few sensor locations and it can be seen that this objective has been reached. As a result, the frequency content and damping characteristics of the measured signals are also reproduced with good accuracy. Finally, we mention that the correlation illustrated in Figure 18 is within the range of experimental uncertainty inferred from the multiple test data sets.

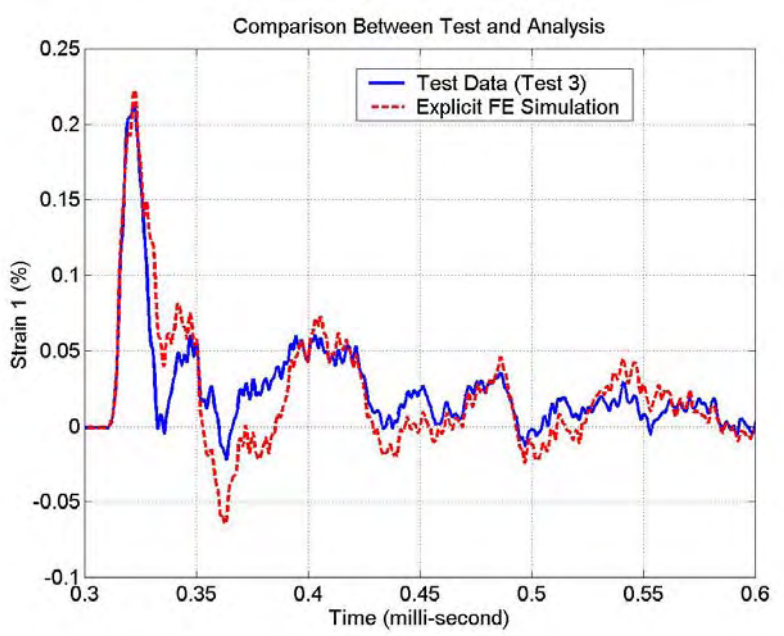

Figure 18. Correlation between measured and predicted responses.

It is emphasized that these results are preliminary. The impulse testbed is not discussed further in the following because it is currently being analyzed in more detail. In particular, more testing is planed in the near future to characterize the response of the system under various excitations (modal testing; impulse testing) and input levels.

4. ASSESSMENT OF MODEL UPDATING TECHNIQUES

In the review of model updating techniques presented in this Section, the discussion is focused around methods that can: 1) handle any type and source of nonlinearity; and 2) enable both parametric and non-parametric updating to be carried out simultaneously. Very few techniques have been found in the published literature that could meet these constraints. As an illustration of this lack of techniques relevant to the nonlinear world, the reader is invited to review from References [9-10] the state-of-the-art in model updating technology. Among the earliest and most promising work in test-analysis correlation for nonlinear dynamics, we cite the work by Hasselman, Anderson and Wenshui [11] and the work by Dippery and Smith [12].

4.1. THEORY

Generally, parametric optimization is achieved by minimizing a “distance” between test data and predictions of the numerical model, whether this distance is evaluated in the time or frequency domain. The optimization problem can be formulated as the minimization of the cost function shown in equation (3) where the first contribution represents the metric used for test-analysis correlation and the second serves the purpose of regularization

$$\min_{\{\delta \mathbf{p}\}} \sum_{j=1 \cdots N_{test}} \{\mathbf{R}_j(\mathbf{p}+\delta\mathbf{p})\}^* \left[\mathbf{S}_{RR_j}\right]^{-1} \{\mathbf{R}_j(\mathbf{p}+\delta\mathbf{p})\} + \{\delta\mathbf{p}\}^T \left[\mathbf{S}_{pp}\right]^{-1} \{\delta\mathbf{p}\} \tag{3}$$

Constraints such as $\mathbf{p}_{min} \le (\mathbf{p}_e + \delta\mathbf{p}_e) \le \mathbf{p}_{max}$ are added to the formulation to filter out local minima that would not be acceptable from a physical standpoint. In the test discussed in Section 4.3 for example, the parameters of interest $\{\mathbf{p}\}$ are the seven spring stiffness parameters allowed to vary of +/-30% about their nominal value. Weighting matrices in equation (3) are generally kept constant and diagonal for computational efficiency. They can also be defined as covariance matrices which formulates a Bayesian correction procedure, as shown in Reference [3]. The only real difficulty is then to track the evolution of the covariance coefficients as parameters in the model are adjusted.

Obviously, many choices for the metric $\{\mathbf{R}_j(\mathbf{p})\}$ are available, the simplest of all being the difference between test and analysis modal parameters. It is also known in the model updating community as the output error residue, see Reference [13], because quantities being compared are outputs as opposed to the excitation inputted to the system

$$\{\mathbf{R}_j(\mathbf{p})\} = \begin{Bmatrix} \omega_1^{test} - \omega_1(\mathbf{p}) \\ \vdots \\ \omega_j^{test} - \omega_j(\mathbf{p}) \\ \phi_{11}^{test} - \phi_{11}(\mathbf{p}) \\ \vdots \\ \phi_{ij}^{test} - \phi_{ij}(\mathbf{p}) \end{Bmatrix} \tag{4}$$

Formulations based on optimization problems may not be as efficient as other approaches, such as formulating the adjoint problem [14], but they offer some advantages besides constituting the overwhelming majority of inverse problem solving techniques. Among others, the formulation (3) is independent of the set of partial differential equations or numerical solver used, independent of the optimization solver and defined only by the choice of metric $\{\mathbf{R}_j(\mathbf{p})\}$. Nevertheless, it is shown in Section 5 that more relevant inverse problem solving strategies are available when the correlation takes place in the time domain.

4.2. LINEAR MODEL UPDATING STRATEGIES

In addition to using the output residue documented in many publications among which we cite Reference [13], the results summarized in Section 4.3 below involve the definition of the force and hybrid modal residues defined in References [15] and [16], respectively. The first one is referred to as a “force” vector because it estimates the out-of-balance forces obtained when the (erroneous) model fails to match the measured dynamics

$$\{\mathbf{R_j(p)}\} = \left([\mathbf{K(p)}] - (\omega_j^{test})^2 [\mathbf{M(p)}]\right)\{\phi_j^{test}\} \tag{5}$$

The second one is referred to as a "hybrid" vector and it can be explained, in a simplified version, as being the displacement field produced by applying the force vector (5) to the static system. It can be defined as

$$\{\mathbf{R_j(p)}\} = \{\varphi_j^{test}\} - \{\varphi_j\} \tag{6}$$

where vector $\{\varphi_j\}$ is obtained by solving the following static system

$$[\mathbf{K(p)}]\{\varphi_j\} = (\omega_j^{test})^2 [\mathbf{M(p)}]\{\phi_j^{test}\} \tag{7}$$

The actual hybrid modal residue can handle incomplete measurements as well as noisy data. Reference [16] offers a complete derivation and addresses some of the implementation concerns. Clearly, the residue vectors (5) and (6) are dual and both vanish when the FE model reproduces the measured data with accuracy. The first metric offers the advantage of being very easy to compute and the second one features nice properties in terms of numerical conditioning. The important issue of incomplete measurement which may introduce a mismatch between sensor locations and degrees of freedom of the model is addressed in both References [15] and [16]. An alternative to dealing with the problem of spatial incompleteness is to apply model reduction and the three metrics (4-6) accommodate condensation techniques with no difficulty. We emphasize that our purpose is not to compare various figures of merit for their efficiency to identify sources of modeling error but rather to illustrate the danger of modal-based updating when the system is characterized by a source of nonlinearity not accounted for by the numerical model. Here, for example, friction in the LANL 8-DOF system is not represented. Although the linear model provides a good agreement with test data before and after parametric correction, the update fails to yield a positive identification of damage.

4.3. VALIDATION OF MODAL-BASED METRICS

To illustrate that modal parameters are unable to characterize nonlinear dynamics properly, the numerical model associated with the LANL 8-DOF system is refined using three different cost functions based on metrics (4-6). The objective of this test is to make the updated, linear model match the identified mode shapes and frequencies with a better degree of confidence than the one illustrated in Table 1. In doing so, the main modeling error (a 14% stiffness reduction located at the fifth spring) should be identified. Each time, the seven stiffness parameters are optimized based on modal parameters extracted from the acceleration data. Measurements are assumed to be available at locations 1, 4 and 7 only and the mismatch between the identified and numerical mode shapes is

resolved using the modal expansion procedure relevant to each metric. To decouple the definition of test-analysis correlation metrics from algorithmic considerations, several optimization solvers are used to minimize the three cost functions. In this study, the order-0 Simplex algorithm, the order-1 conjugate gradient algorithm and the order-2 BFGS and Levenberg-Marquardt methods are implemented. These classical solvers are described in many publications and manuscripts among which we cite Reference [17].

A typical correlation after updating is illustrated in Table 3. It shows that the original frequency errors have been reduced to very small amounts and that the correlation of mode shape vectors has been improved. Based on such good correlation, most analysts would agree on the success of the updating procedure. However, the adjustment brought to each of the spring stiffness values in Figure 19 proves it impossible to identify the precise location and extent of structural damage. Worse, false positives (that is, stiffness reductions predicted at locations where no damage was originally introduced) are obtained. In the context of a practical engineering application, such false positives would result into a wrong diagnosis and/or erroneous stress predictions.

Table 3. Test-analysis correlation of the LANL 8-DOF testbed for nonlinear vibrations.
(Correlation between the damaged, linear system and the adjusted linear model.)

Mode Number	Identified Frequency	FE Model Frequency	Modal Assurance Criterion (MAC)	Frequency Error
1	22.3 Hz	22.4 Hz	99.9%	0.3%
2	43.9 Hz	44.2 Hz	99.9%	0.6%
3	64.8 Hz	65.9 Hz	98.2%	1.7%
4	85.9 Hz	85.1 Hz	97.2%	-0.9%
5	99.7 Hz	99.8 Hz	99.6%	-0.1%

The top half of Figure 19 illustrates the correction brought to each of the seven springs when the force residue metric (5) is implemented. Similarly, results of the hybrid residue metric (6-7) are shown on the bottom half of Figure 19. The correlation listed in Table 3 corresponds to metric (5) and similar trends are obtained with metric (6-7). The output error residue (4) fails to provide any meaningful model and these results are not commented further.

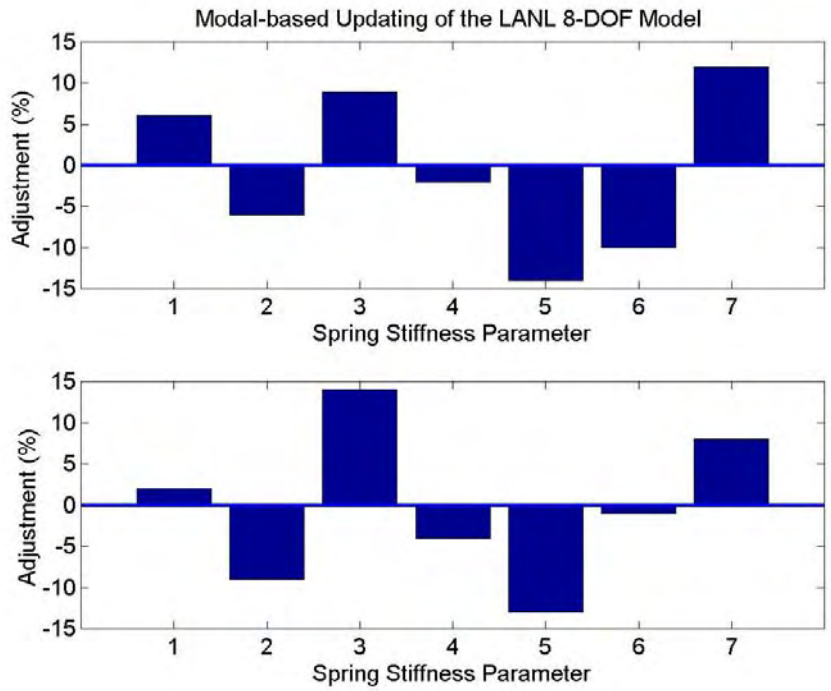

Figure 19. Adjustment brought to the spring stiffness parameters of the LANL 8-DOF model.
(Top: force modal residues (5) are minimized; Bottom: hybrid modal residues (6-7) are minimized.)

We conclude from these results that situations may arise where modal-based metrics fail to estimate the "true" correlation between two data sets when one of them or both represent a nonlinear system. In the example presented, the three metrics considered seem to indicate that various models match the test data when, in fact, the actual modeling error is not identified. Since various optimization solvers were implemented, we believe that these poor results are to blame on the metrics themselves and not on potential convergence difficulties. Our conclusion illustrates the need to define other metrics. Next, test-analysis correlation based on time series is discussed.

4.4. TIME-DOMAIN CORRELATION METRICS

Two time-domain metrics are introduced briefly. The first one correlates the measured and simulated signals directly while the second one correlates the subspaces to which these signals belong. This is achieved by making the numerical model match the singular values and vectors obtained by decomposition of the test data matrix, a procedure generally referred to as Principal Component Decomposition (PCD). Reference [11] offers a complete description of this procedure. This presentation is not intended as an exhaustive discussion of time-domain metrics. Obviously, many choices are possible depending on the application targeted. Our purpose is to introduce the main correlation indicators and to assess their efficiency using the LANL 8-DOF testbed defined in Section 3.

For clarity, we assume that the system of interest is modeled by a set of partial differential equations that can be integrated in time to provide the time-history of various state variables. In structural dynamics, the second-order equation of motion is described by

$$[\mathbf{M(p)}]\left\{\frac{\partial^2 \mathbf{x(p,t)}}{\partial \mathbf{t}^2}\right\} + [\mathbf{K(p)}]\{\mathbf{x(p,t)}\} + \{\mathbf{F_{int}(p,t)}\} = \{\mathbf{F_{ext}(t)}\} \tag{8}$$

Equation (8) states that the system is in equilibrium when the applied loading in the right-hand side matches the combination of inertia and internal forces in the left-hand side. The nonlinear internal force vector $\{\mathbf{F_{int}(p,t)}\}$ accounts for any nonlinear function of the system's state variables. Since the numerical model can be parametrized by a set of design variables $\{\mathbf{p}\}$, time-domain responses such as the position vector $\{\mathbf{x(p,t)}\}$ are shown to depend implicitly on these parameters. Next, we assume that time-varying quantities denoted by $\{\mathbf{u(t)}\}$ are obtained from the state variables. These can represent arbitrary combinations of displacement, velocity and acceleration or any other quantity (strain, pressure, etc.) that may be needed for engineering analysis. In the example below, acceleration data are employed. Since our objective is to generate a more accurate model, the simplest and most natural metric is the Root Mean Square (RMS) error between test and simulation data. The corresponding residue vectors are defined as

$$\{\mathbf{R(t)}\} = \{\mathbf{u^{test}(t)}\} - \{\mathbf{u(p;t)}\} \tag{9}$$

The computational procedure consists of the following steps: 1) For a parametric model defined by a design $\{\mathbf{p}\}$, the FE response is simulated via numerical integration of equation (8); 2) Residues (9) are calculated at prescribed degrees of freedom and time samples; and 3) The cost function $\mathbf{J(p)}$ is optimized where

$$\mathbf{J(p)} = \sum_{\mathbf{j}=1\cdots \mathbf{N_t}} \sum_{\mathbf{i}=1\cdots \mathbf{N_s}} \left(\mathbf{u_i^{test}(t_j)} - \mathbf{u_i(p;t_j)}\right)^2 + \alpha \sum_{\mathbf{k}=1\cdots \mathbf{N_p}} \left(\mathbf{p_k} - \mathbf{p_k^{nominal}}\right)^2 \tag{10}$$

For simplicity, equation (10) assumes a deterministic form. Nevertheless, generalization to a recursive Bayesian formulation offers no difficulty provided that the covariance matrices can be updated at low computational cost.

The PCD method validated in Reference [11] and Reference [18], among others, generalizes the notion of mode shape for nonlinear systems. Rather than using a direct comparison between time series, test and simulation data are first assembled into matrices

$$[\mathbf{U}(\mathbf{t_i}:\mathbf{t_f})]=\begin{bmatrix} \mathbf{u_1}(\mathbf{t_i}) & \mathbf{u_1}(\mathbf{t_{i+1}}) & \cdots & \mathbf{u_1}(\mathbf{t_f}) \\ \mathbf{u_2}(\mathbf{t_i}) & \mathbf{u_2}(\mathbf{t_{i+1}}) & \cdots & \mathbf{u_2}(\mathbf{t_f}) \\ \vdots & \vdots & \ddots & \vdots \\ \mathbf{u_{N_o}}(\mathbf{t_i}) & \mathbf{u_{N_o}}(\mathbf{t_{i+1}}) & \cdots & \mathbf{u_{N_o}}(\mathbf{t_f}) \end{bmatrix} \tag{11}$$

Then, the subspaces spanned by the rows (or columns) of such test and analysis, rectangular matrices are estimated using a Singular Value Decomposition (SVD) expressed in terms of left, orthogonal singular vectors $\{\Phi_j\}$, right, orthogonal singular vectors $\{\Psi_j\}$ and singular values σ_j

$$[\mathbf{U}^{\mathbf{test}}]=[\Phi^{\mathbf{test}}][\Sigma^{\mathbf{test}}][\Psi^{\mathbf{test}}]^{\mathrm{T}}, \qquad [\mathbf{U(p)}]=[\Phi\mathbf{(p)}][\Sigma\mathbf{(p)}][\Psi\mathbf{(p)}]^{\mathrm{T}} \tag{12}$$

Finally, the cost function used for optimizing the model's parameters $\{\mathbf{p}\}$ is defined as a combination of the distance between the pseudo-subspaces (represented by the left singular vectors $\{\Phi_j\}$), the energy difference of each signal (represented by the singular values σ_j) and the error in time series (represented by the right singular vectors $\{\Psi_j\}$)

$$\mathbf{J(p)}=\frac{\mathbf{1}}{\mathbf{N_o^2}}\|\delta\Phi\mathbf{(p)}\|_2^2+\frac{\mathbf{1}}{\mathbf{N_o}}\|\delta\Sigma\mathbf{(p)}\|_2^2+\frac{\mathbf{1}}{\mathbf{N_oN_t}}\|\delta\Psi\mathbf{(p)}\|_2^2+\alpha\left\|\mathbf{p}-\mathbf{p}^{\mathbf{nominal}}\right\|_2^2 \tag{13}$$

where the normalized errors between test and analysis components of the SVD's are defined as

$$\begin{aligned} [\delta\Phi\mathbf{(p)}] &= [\Phi^{\mathbf{test}}]^{\mathrm{T}}[\Phi\mathbf{(p)}]-[\mathbf{I}] \\ [\delta\Sigma\mathbf{(p)}] &= [\Sigma^{\mathbf{test}}]^{-1}([\Sigma^{\mathbf{test}}]-[\Sigma\mathbf{(p)}]) \\ [\delta\Psi\mathbf{(p)}] &= [\Psi^{\mathbf{test}}]^{\mathrm{T}}[\Psi\mathbf{(p)}]-[\mathbf{I}] \end{aligned} \tag{14}$$

Since the singular vectors are orthogonal, they provide a time-varying basis of the multi-dimensional manifolds to which the nonlinear signals belong [19]. In addition, the SVD offers a practical way of filtering out any measurement noise or rigid-body mode contribution because these are typically associated with singular values much smaller than those characteristic of the dynamics. However, we emphasize that the SVD alone can generally not be used for detecting the presence of a nonlinearity.

4.5. VALIDATION OF TIME-DOMAIN METRICS

The results are briefly discussed of applying the PCD time-domain correlation metric to a test data set collected using the LANL 8-DOF testbed. This illustration consists of locating structural damage with a linear configuration of the system. The configuration used for this example is identical to the one described in Section 3.3

(same linear system, sensing configuration and damage scenario). The only difference is that the PCD cost function is now implemented instead of modal data. The results can be compared with those of Section 4.3 (see Figure 19).

The updating procedure implemented performs an optimization of the (constant) design parameters when a set of incomplete, time-domain measurements are provided. Only acceleration outputs at locations 1, 5 and 6 are assumed available. In addition to updating the model's seven spring stiffness parameters, the procedure also optimizes the eight time-varying components of the internal force vector $\{\mathbf{F}_{\text{int}}(\mathbf{p},\mathbf{t})\}$ in equation (8). The reason for optimizing the internal force vector is because our original model does not account for any source of nonlinearity that we know to be affecting the measurements (friction, "stick and slip," etc.). The overall procedure goes as follows. Unknowns of the optimization are the seven spring stiffness parameters and eight force components. The PCD correlation is based on the first 90 acceleration measurements at sensors 1, 5 and 6 that span a [0;0.168] second time window. For the numerical simulation, the FE matrices and force vectors are reduced to the size of the test model (locations 1, 5 and 6 only) and the response of the condensed model is integrated in time using 10 sampling points between any two measurements. As the response is integrated in time, the stiffness values and internal force vector are optimized. A total of 89 optimizations are therefore carried out in the time window [0;0.168] second. After a few optimizations, the spring stiffness parameters converge to the values shown below. No clear interpretation of the identified forcing function (nonlinear term) can be made and these results are not further discussed here.

The adjustment brought to the seven springs is represented in Figure 20 in percentage of the original stiffness value. The only spring that witnesses a significant reduction is the fifth one, as expected. In addition, the 17% loss of stiffness predicted is in very good agreement with the 14% reduction inflicted during the test. The stiffening of springs 1, 2 and 6 can not be explained other than by evoking the implicit least-squares nature of the solution procedure that tends to smear the adjustment throughout the set of parameters. Nevertheless, these corrections remain small in magnitude and inconsistent with a damage. As mentioned previously, we believe that friction plays an important role in the dynamics of the mass/spring system. The reason is that large modal damping ratios (over 10%) are identified from the test data which is inconsistent with the oscillations observed (the acceleration response does not feature an exponential decay anywhere comparable to 10%). The fact that friction is not accounted for in the numerical model may also contribute to the distortion of the solution.

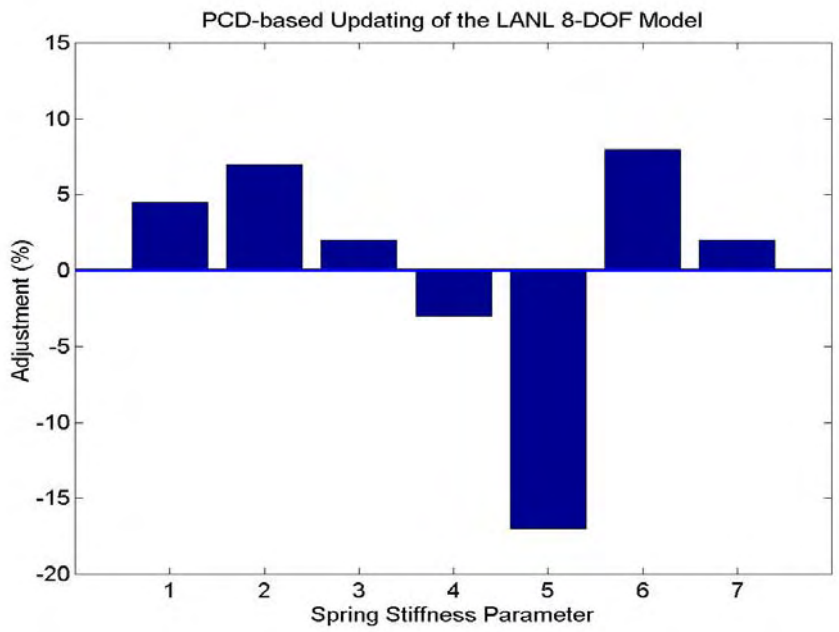

Figure 20. Adjustment brought to the spring stiffness parameters of the LANL 8-DOF model. (The PCD time-domain cost function (13) is minimized.)

This example illustrates that time-domain metrics outperform modal-based metrics when the dynamics investigated is significantly nonlinear and/or modal parameters are not well suited to its description. They however introduce problems of their own that are addressed in Sections 5 and 6.

5. OPTIMAL ERROR CONTROL

One problem of time-domain model validation that has not been addressed previously is the reconstruction of continuous solution fields during the optimization. This issue is fundamental because, if the inverse problem is not formulated correctly, the numerical model yields discontinuous acceleration, velocity and displacement fields which contradicts the laws of mechanics for the class of problems investigated here. After explaining where discontinuous solution fields originate from, a new formulation of the inverse problem in the time domain is proposed. It is based on the theory of optimal control, as explained in References [12] and [20], and relies on the resolution of multiple two-point Boundary Value Problems (BVP). When satisfactory solutions to the two-point BVP's are obtained, the numerical model is guaranteed to match the measured data at the beginning and at end of the time window considered. We emphasize that the idea of optimal error control is not an original one. Full credit must be given to the authors of References [12] and [20] although their motivation was somewhat different. Our contribution is to provide a complete derivation of the algorithm which is needed for the discussion in Section 5.5.

5.1. DISCONTINUITY OF THE SOLUTION FIELDS

The strategy of implementing successive optimizations produces several optimized models, one for each time window considered. This is necessary not only for computational purposes but also because some of the parameters being optimized may vary in time and following such evolution as it is occurring may be critical to model validation. However, nothing in the formulation of the inverse problem enforces continuity between the solution fields obtained from models optimized within the i^{th} and $(i+1)^{th}$ time windows. Since the optimization variables can converge to different solutions $\{p^{(i)}\}$ and $\{p^{(i+1)}\}$ in two successive time windows, the discontinuity of the solution can be written, for example, in terms of the displacement field as

$$\lim_{\substack{t \to t_i \\ t \le t_i}} x(p^{(i)}, t) \neq \lim_{\substack{t \to t_i \\ t \ge t_i}} x(p^{(i+1)}, t) \tag{15}$$

In the following, it is explained how optimal control strategies can be implemented to solve the inverse test-analysis correlation problem while reconstructing continuous solution fields and identifying the source of modeling error. An application to a single degree of freedom system shows that the optimal control approach does indeed resolve the discontinuity but also that practical applications remain out-of-reach because of the extreme computational requirement of the algorithm.

5.2. TEST-ANALYSIS CORRELATION VIA OPTIMAL ERROR CONTROL

For clarity, the evolution of the system investigated is recast as a set of first-order partial differential equations. In structural dynamics, this would typically be achieved using the state-space form. We emphasize that the first-order formulation is used for simplicity only; the algorithm can be implemented in terms of second-order systems if computational efficiency dictates so, as we show in Section 5.3. Our starting point is a time-domain solver that provides a solution $\{x(t)\}$ to the set of nonlinear equations

$$\left\{\frac{\partial x}{\partial t}(t)\right\} = \{F(p, x, t)\} + \{e(t)\} \tag{16}$$

In equation (16), vector $\{e(t)\}$ represents the contribution of a generic modeling error. It includes everything that the numerical model does not account for. It is important to realize how general this definition is: the error contribution can be defined as a combination of modeling errors, discretization errors, etc., but it can also account for experimental or numerical variability. We also introduce the notation $\{y(t)\}$ that represents a vector of features, that is, quantities obtained from the solution vectors $\{x(t)\}$ and that can also be assessed from the measurements.

This vector can, for example, represent an arbitrary combination of acceleration and pressure data at various locations.

The inverse problem is re-formulated as follows. The objective is to reconstruct continuous time series such as $\{x(t)\}$ in such a way that the features in $\{y(t)\}$ match the test data. Simultaneously, the procedure must provide a parametric adjustment of the model's design variables $\{p\}$ and identify the unknown, non-parametric error $\{e(t)\}$. For simplicity, the cost function is formulated as the RMS error between test and simulated data but it can be verified that any cost function may be used instead. Since the unmodeled dynamics plays a role identical to that of a controller in the theory of optimal control, a "minimum effort" penalty term must be added to avoid generating unrealistic error levels. Hence, the basic cost function can be stated as

$$J(p) = \sum_{k=1\cdots N_t} \left(\{y^{test}(t_k)\} - \{y(p,t_k)\}\right)^T [S_{yy}(t_k)]^{-1} \left(\{y^{test}(t_k)\} - \{y(p,t_k)\}\right) + \sum_{k=1\cdots N_t} \{e(t_k)\}^T [S_{ee}(t_k)]^{-1} \{e(t_k)\} \quad (17)$$

The resolution procedure is a direct application of the theory of optimal control. First, the cost function (17) is augmented with the evolution equation (16). This is achieved by introducing a vector $\{\lambda(t)\}$ of Lagrange multipliers (also referred to as the system's "co-state" variables) that penalize the total cost in the event where the state equation is not satisfied. The augmented cost function is defined as

$$\begin{aligned} \bar{J}(p;x;e) = & \sum_{k=1\cdots N_t} \left(\{y^{test}(t_k)\} - \{y(p,t_k)\}\right)^T [S_{yy}(t_k)]^{-1} \left(\{y^{test}(t_k)\} - \{y(p,t_k)\}\right) \\ & + \sum_{k=1\cdots N_t} \{e(t_k)\}^T [S_{ee}(t_k)]^{-1} \{e(t_k)\} - \{\lambda(t_k)\}^T \left(\left\{\frac{\partial x}{\partial t}(t_k)\right\} - \{F(p;x;t_k)\} - \{e(t_k)\} \right) \end{aligned} \quad (18)$$

Adding a set of variables $\{\lambda(t)\}$ may seem inconsistent with the objective of simplifying the resolution procedure. The reason is that these new unknowns provide additional equations that can be solved for to ensure that the numerical solution matches the test data at the beginning and at the end of each time window. The numerical algorithm is obtained in a classical manner by: 1) converting $\bar{J}$ into a continuous functional; 2) performing an integration over the time window $[t_i;t_{i+1}]$ considered; and 3) applying the necessary conditions $\frac{\partial \bar{J}}{\partial x} = 0$ and $\frac{\partial \bar{J}}{\partial e} = 0$. It yields the following set of governing equations that must be solved simultaneously in each time window $[t_i;t_{i+1}]$

$$
\begin{aligned}
&\{\dot{\mathbf{x}}(\mathbf{t})\} = \{\mathbf{F}(\mathbf{p},\mathbf{x},\mathbf{t})\} + \{\mathbf{e}(\mathbf{t})\} \\
&\{\dot{\lambda}(\mathbf{t})\} = -\left[\frac{\partial \mathbf{F}}{\partial \mathbf{x}}(\mathbf{p};\mathbf{x};\mathbf{t})\right]^{\mathbf{T}} \{\lambda(\mathbf{t})\} \\
&\{\mathbf{e}(\mathbf{t})\} = -\frac{\mathbf{1}}{\mathbf{2}}[\mathbf{S}_{\mathbf{ee}}(\mathbf{t})]\{\lambda(\mathbf{t})\} \\
&\{\lambda(\mathbf{t}_\mathbf{k}^+)\} = \{\lambda(\mathbf{t}_\mathbf{k}^-)\} + \mathbf{2}\left[\frac{\partial \mathbf{y}}{\partial \mathbf{x}}(\mathbf{p},\mathbf{t}_\mathbf{k})\right]^{\mathbf{T}} [\mathbf{S}_{\mathbf{yy}}(\mathbf{t}_\mathbf{k})]^{-1}\left(\{\mathbf{y}^{\mathbf{test}}(\mathbf{t}_\mathbf{k})\} - \{\mathbf{y}(\mathbf{p},\mathbf{t}_\mathbf{k})\}\right) \\
&\{\mathbf{x}(\mathbf{t}_\mathbf{i})\} = \{\mathbf{x}^{\mathbf{test}}(\mathbf{t}_\mathbf{i})\} \mathbf{or} \{\lambda(\mathbf{t}_\mathbf{i}^-)\} = \mathbf{0} \\
&\{\mathbf{x}(\mathbf{t}_{\mathbf{i+1}})\} = \{\mathbf{x}^{\mathbf{test}}(\mathbf{t}_{\mathbf{i+1}})\} \mathbf{or} \{\lambda(\mathbf{t}_{\mathbf{i+1}}^+)\} = \mathbf{0}
\end{aligned}
\tag{19}
$$

It can be observed that the fourth equation above represents the discontinuity of the co-states. As expected, it is shown to be a direct consequence of how well test data are reproduced by the numerical model. To the extent where the observation vector matches the test data exactly, no discontinuity is propagated to the co-states. The last two of equations (19) ensure that the test data are reproduced at the beginning and at the end of each time window. The only remaining step is to integrate this procedure to a parametric optimization solver. The solver itself may be any "black box" optimizer that the user finds convenient to implement. The basic requirement is that the value of a cost function $J(p)$ be obtained for any arbitrary design $\{p\}$. This calculation is summarized below.

5.3. NUMERICAL IMPLEMENTATION

To illustrate how the optimal control formulation can be applied to structural dynamics, equations are transformed back into their second-order form. The five-step procedure outlined below is encapsulated within the optimization solver. For a given set of variables $\{p\}$, the cost function $J(p)$ defined in equation (17) is calculated by:

Step 1. Choice of the initial condition $\{\lambda_o\}$: Given a particular design $\{p\}$, the co-state's initial condition must be obtained that minimizes the difference between test and numerical data. The cost function to minimize can, for example, be defined as the RMS error

$$
\mathbf{J}(\lambda_\mathbf{o}) = \sum_{\mathbf{k=i,i+1}} \left(\{\mathbf{y}^{\mathbf{test}}(\mathbf{t}_\mathbf{k})\} - \{\mathbf{y}(\lambda_\mathbf{o},\mathbf{t}_\mathbf{k})\}\right)^{\mathbf{T}} \left(\{\mathbf{y}^{\mathbf{test}}(\mathbf{t}_\mathbf{k})\} - \{\mathbf{y}(\lambda_\mathbf{o},\mathbf{t}_\mathbf{k})\}\right) \tag{20}
$$

This optimization problem introduces the two-point boundary value problem mentioned previously because, once the optimum is found, the observation vector is guaranteed to match test data at the time increments considered. The optimization problem defined by the cost function (20) would typically be embedded into the outer parametric optimization loop. In addition, calculating the feature $\{y(\lambda_o,t)\}$ for a given initial condition $\{\lambda_o\}$ requires the evaluation of Steps 2-5 below which renders the entire procedure extremely time-consuming.

Step 2. Time integration for the co-state: Once the initial condition has been optimized to ensure continuity of the solution fields, the co-state equation (19) is integrated. The equivalent second-order form is

$$[M(p)]\left\{\frac{\partial^2\lambda(t)}{\partial t^2}\right\}+[K(p)]\left\{\frac{\partial\lambda(t)}{\partial t}\right\}=0 \tag{21}$$

Note that this system is unstable: it can be verified that some of its eigenvalues are complex with a positive real part. Very short time windows $[t_i;t_{i+1}]$ must therefore be considered so that oscillations do not have time to grow unstable. The obvious inconvenient is that shorter windows require more two-point BVP's to be solved.

Step 3. Reconstruction of the non-parametric, unmodeled dynamics:

$$\{e(t)\}=-\frac{1}{2}[S_{ee}(t)]\{\lambda(t)\} \tag{22}$$

Step 4. Integration of the equation of motion: The second-order equation of motion is integrated with the contribution of the modeling error identified at Step 3 and starting with the initial condition $\{x(t_i)\}=\{x^{test}(t_i)\}$ and $\{\dot{x}(t_i)\}=\{\dot{x}^{test}(t_i)\}$

$$\mathbf{[M(p)]\{\ddot{x}(t)\}+[K(p)]\{x(t)\}+\{F_{int}(p,t)\}=\{F_{ext}(t)\}+\{e(t)\}} \tag{23}$$

Adding the error term in equation (23) guarantees that the displacement, velocity and acceleration fields match the measured data at the end of the current time window, $\mathbf{t_i=t_{i+1}}$. Potential discontinuities are "absorbed" by the co-state and error variables. Note that the tolerance used for monitoring the convergence of the two-point BVP (20) defines the maximum allowed discontinuity of the solution fields. A trade-off between the continuity constraint and the computational requirement can therefore be achieved.

Step 5. Calculation of the cost function: Finally, the feature vector $\{y(t)\}$ is estimated using the solution fields obtained by integrating equation (23). The cost function $J(p)$ is calculated from one of the definitions (10) or (13) or any other if more appropriate metrics can be defined.

So far, the choice of matrices $[S_{yy}(t)]$, $[S_{ee}(t)]$ and $[S_{pp}(t)]$ (if a minimum-change contribution is added to the cost function) has not been discussed. If kept constant, it is most convenient to adopt diagonal matrices. However, Reference [12] reports that the selection of weights in $[S_{ee}(t)]$ can be critical to the overall convergence, in which case a second inner loop should be implemented to adjust these weights as needed. The weighting can also be

defined in terms of covariance matrices for implementing a maximum likelihood approach or a Bayesian parameter identification method. Variance and covariance data in matrix $[S_{yy}(t)]$ are obtained directly from test data. Similarly, variance and covariance data in matrix $[S_{pp}(t)]$ are derived from the model's uncertainty characterization. The only computational difficulty is the evaluation and updating of the error covariance matrix $[S_{ee}(t)]$. The analyst must generally compromise between computational efficiency (that favors uncorrelated statistics and diagonal matrices) and accuracy (that requires higher-order approximations and multiple matrix factorizations).

To illustrate the optimal error control approach, a numerical example is presented that involves forced vibrations of the single-degree of freedom Duffing oscillator. This simple, nonlinear system provides a good understanding of the method's capability and limitation, as discussed below.

5.4. NUMERICAL ILLUSTRATION USING A SINGLE DEGREE OF FREEDOM SYSTEM

To illustrate how the optimal control algorithm works for solving an inverse test-analysis correlation problem, the Duffing oscillator presented in Section 3.1 is investigated. First, the set of equations (1) is integrated in time to generate the so-called reference data in the [0;30] second window. Two "experimental" data sets are obtained by sampling the reference data and adding noise to the discrete measurements. The first set of displacement and velocity measurements consists of 11 points while the second set consists of 151 points. The noise introduced in both cases is Gaussian with a noise-to-signal ratio set to 5%. Then, the internal force is removed. Therefore, the starting model is linear and the (unknown) modeling error is simply $e(t) = F_{int}(t)$. Ten successive optimization windows $[t_i ; t_{i+1}]$ are defined over the 30 second time period and a total of 75 increments are used for integrating the solution within each window. The feature vector $\{y(t)\}$ considered collects the displacement and velocity "measurements" at the 11 (respectively, 151) samples t_i where test data are assumed available. The inverse problem is first solved using the set of 11 measurements, then a second resolution is performed using the set of 151 measurements. Both results are compared below. In both cases, the error weighting matrix is kept constant with weights equal to one half

$$\left\{\mathbf{y}^{\mathbf{test}}(\mathbf{t}_i)\right\} = \begin{Bmatrix} \mathbf{x}^{\mathbf{test}}(\mathbf{t}_i) \\ \dot{\mathbf{x}}^{\mathbf{test}}(\mathbf{t}_i) \end{Bmatrix}, \quad \left\{\mathbf{y}(\mathbf{p}, \mathbf{t}_i)\right\} = \begin{Bmatrix} \mathbf{x}(\mathbf{p}, \mathbf{t}_i) \\ \dot{\mathbf{x}}(\mathbf{p}, \mathbf{t}_i) \end{Bmatrix}, \quad \left[\mathbf{S}_{\mathbf{ee}}(\mathbf{t}_k)\right] = \begin{bmatrix} \mathbf{0.5} & \mathbf{0} \\ \mathbf{0} & \mathbf{0.5} \end{bmatrix} \tag{24}$$

Figure 21 illustrates the correlation of the updated models. The procedure outlined in Section 5.3 identifies the internal force as a function of time and this result is shown in Figure 22. It can be observed from Figure 21 that the optimized models are in good agreement with reference data especially when the test-analysis correlation is based on 151 samples. The dashed lines that represent the response of the models after optimization provide a significant improvement over the original response in Figure 2. We emphasize that only the 11 or 151 sampling points are used

to fit the model; the baseline, noise-free solution pictured by the solid line is shown only for the purpose of assessing whether or not the models reproduce the continuous solution. This example illustrates that correlated models can generate continuous displacement, velocity and acceleration fields even though ten successive optimizations are carried out independently from one another.

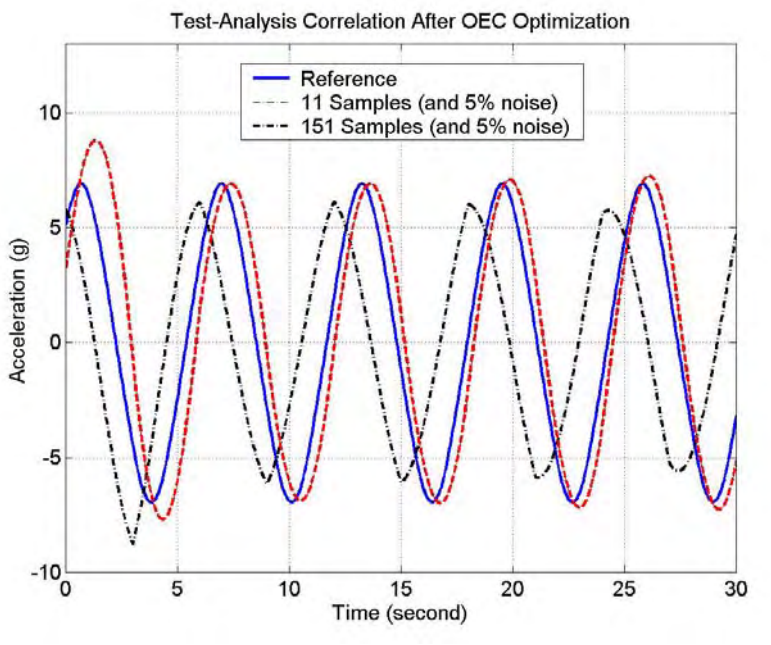

Figure 21. Test-analysis correlation of the single degree of freedom system after model updating.

When analyzing the solution obtained from 11 measurements, it can be concluded from Figure 22 that the error identified from this procedure approaches the "true" cubic nonlinearity with a fair accuracy. Both the periodicity and overall amplitude of the nonlinear force are captured. At the very least, this solution could provide some insight into the nature of the nonlinearity and the approximate value of the nonlinear spring. For example, if a simple parametric model such as $e(t) = \alpha\left(x^3(t)\right)$ is curve-fitted in the least-squares sense to the values of $e(t)$ obtained in Figure 22, the nonlinear spring stiffness is estimated to be equal to $\alpha = 0.065$ instead of the value $k_{nl} = 0.05$ used (30% error). Since the error vector is estimated directly from the co-states in equation (22), discontinuities obtained when the solution progresses from one time window to the next are visible in Figure 22. The theory of optimal control states that the controller becomes continuous if an infinite number of observations are available. For our application, this means that the error vector should converge to the "true" error if more measurements are available. This is verified in Figure 22. For the case where 151 measurements are available instead of the previous 11, it shows that the optimal error control delivers a very accurate estimation of the unknown dynamics. A direct result is that the displacement, velocity and acceleration fields predicted by the optimized models, while remaining continuous, match the test data with even greater accuracy.

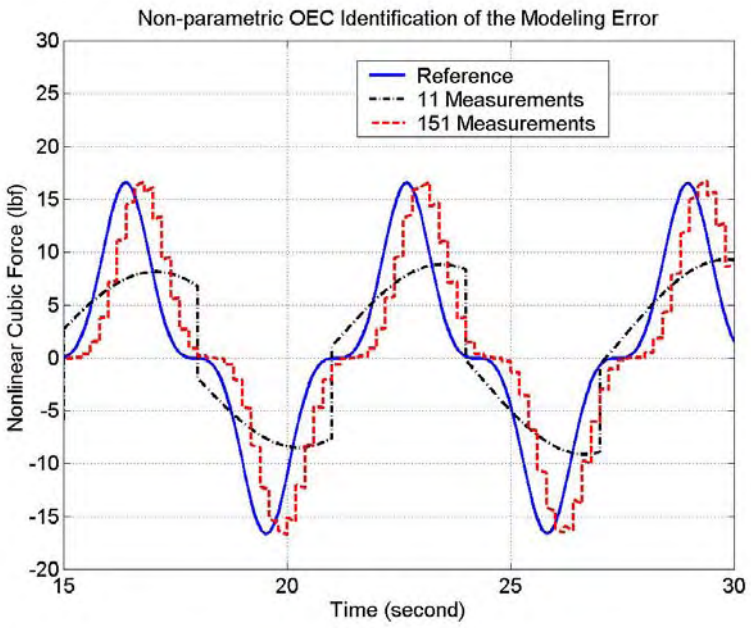

Figure 22. Non-parametric identification of the modeling error with the single degree of freedom system.

5.5. DISCUSSION OF THE RESULTS

The important conclusion that we emphasize in this Section is that extreme care must be brought to the formulation of model validation when time series are employed. Unconstrained optimization may result in discontinuous solution fields. This difficulty can be alleviated by formulating an optimal controller of the modeling error. This is a very attractive technique because not only does it handle parametric and non-parametric identifications simultaneously but it also propagates uncertainty using the Bayesian theory of information and it provides a rigorous framework for generating continuous solutions from an arbitrary number of optimizations.

However, this improvement comes with the additional cost of formulating a two-point BVP to guaranty continuity of the solution. Since the procedure is embedded within an optimization solver, multiple two-point BVP's must be solved for. Unfortunately, the impact on the computational requirement is enormous. For example, solving the Duffing oscillator problem requires a total of 16 to 20 hours of CPU time depending on the number of measurement points available. The 4-degree of freedom system shown in Figure 3 was also investigated. This application consisted in calculating the stiffness of each of the four springs and identifying the cubic internal force (assumed unknown). The resolution required about 70 hours of CPU time. These timings were obtained on a dedicated R10,000/250 MHertz RISC processor when the algorithm is programmed within the environment provided by Matlab™. Clearly, these figures prohibit any application of the technique to practical engineering problems. It is for this reason that other avenues must be explored.

6. CONCLUSION

The work presented in this publication addresses the correlation of nonlinear models with test data. One of the specificity is that modal superposition can generally not be considered as a valuable solution technique due to its inability to represent arbitrary nonlinearity and to capture the dynamics of transient events. For this reason, test-analysis correlation must rely on time series. Several testbeds developed at Los Alamos National Laboratory in support of our health monitoring and code validation and verification programs are presented. Their purpose is to provide experimental data for validating the strategies implemented for test-analysis correlation and inverse problem solving. Linear model updating techniques are reviewed and their inefficiency is illustrated using a testbed developed to analyze nonlinear vibrations. Then, time-domain techniques are discussed and applied with greater success. Finally, we show that a careless formulation of the inverse problem in the time domain yields discontinuous solution fields which violates the most basic laws of mechanics. This difficulty is alleviated by formulating an optimal controller of the modeling error. This technique is capable of simultaneously 1) handling parametric and non-parametric identifications; 2) propagating uncertainty and variability using the Bayesian theory of information; and 3) providing a rigorous framework to generate continuous solutions from an arbitrary number of optimizations. Its computational requirement however makes it impractical for solving meaningful engineering problems.

To bypass some of the difficulties identified in this work, our current emphasis is on replacing inverse problems with multiple forward, stochastic problems. After a metric has been defined for comparing test and analysis data, response surfaces are generated that can be used for 1) assessing in a probabilistic sense the quality of a particular simulation with respect to “reference” or test data; and 2) optimizing the model’s design parameters to improve its predictive quality. One critical issue to be investigated in future research is the definition of adequate metrics for correlating transient, nonlinear data. Rather than attempting to define deterministic distances, future work will emphasize dealing with “clusters” of test and analysis data that must be compared in a statistical sense.

To conclude, it is our opinion that test-analysis correlation and inverse problem solving for nonlinear structural dynamics must address the following issues: 1) How to characterize the variability of an experiment/design? 2) How to generate additional or surrogate data sets that can increase the knowledge about the experiment/design? 3) How to select features that best characterize a nonlinear data set? 4) How to assess statistically the consistency between multiple data sets? 5) How to develop fast probability integration capabilities and interface them to our analysis tools? These problems and the overall issue of model validation are further discussed in Reference [21].

REFERENCES

1. Lieven, N.A.J., and Ewins, D.J., "A Proposal For Standard Notation and Terminology in Modal Analysis," *10th SEM International Modal Analysis Conference*, San Diego, California, Feb. 2-5, 1992, pp. 1414-1419.

2. Hemez, F.M., and Doebling, S.W., "Test-Analysis Correlation and Finite Element Model Updating for Nonlinear, Transient Dynamics," *17th SEM International Modal Analysis Conference*, Kissimmee, Florida, Feb. 8-11, 1999, pp. 1501-1510.

3. Hemez, F.M., and Doebling, S.W., "A Validation of Bayesian Finite Element Model Updating for Linear Dynamics," *17th SEM International Modal Analysis Conference*, Kissimmee, Florida, Feb. 8-11, 1999, pp. 1545-1555.

4. Burton, T.D., Hemez, F.M., and Rhee, W., "A Combined Model Reduction/SVD Approach to Nonlinear Model Updating," *18th SEM International Modal Analysis Conference*, San Antonio, Texas, Feb. 7-10, 2000, pp. 116-123.

5. Rhee, W., "Linear and Nonlinear Model Reduction in Structural Dynamics With Application to Model Updating," Doctoral Dissertation, Texas Tech University, Lubbock, Texas, Aug. 2000.

6. **Abaqus/Explicit**, User's Manual, Version 5.8, Hibbitt, Karlsson & Sorensen, Inc., Pawtucket, Rhode Island, 1998.

7. McKay, M., "Sampling Variability of Measures of Input-Variable Importance in Computer Models," *3rd DoE/MICS Workshop on the Predictability of Complex Phenomena*, Los Alamos, New Mexico, Dec. 6-8, 1999.

8. **NESSUS**, User's Manual, Version 2.3, Southwest Research Institute, San Antonio, Texas, 1996.

9. Imregun, M., and Visser, W.J., "A Review of Model Updating Techniques," *Shock and Vibration Digest*, Vol. 23, No. 1, 1991, pp. 19-20.

10. Mottershead, J.E., and Friswell, M.I., "Model Updating in Structural Dynamics: A Survey," *Journal of Sound and Vibration*, Vol. 162, No. 2, 1993, pp. 347-375.

11. Hasselman, T.K., Anderson, M.C., and Wenshui, G., "Principal Components Analysis For Nonlinear Model Correlation, Updating and Uncertainty Evaluation," *16th SEM International Modal Analysis Conference*, Santa Barbara, California, Feb. 2-5, 1998, pp. 664-651.

12. Dippery, K.D., and Smith, S.W., "An Optimal Control Approach to Nonlinear System Identification," *16th SEM International Modal Analysis Conference*, Santa Barbara, California, Feb. 2-5, 1998, pp. 637-643.

13. Piranda, J., Lallement, G., and Cogan, S., "Parametric Correction of Finite Element Models By Minimization of an Output Residual: Improvement of the Sensitivity Method," *9th SEM International Modal Analysis Conference*, Firenze, Italy, Jan. 1991.

14. Hanson, K.M., Cunningham, G.S., and Saquib, S.S., "Inversion Based on Computational Simulations," Maximum Entropy and Bayesian Methods, Erickson, G.J., Rychert, J.T., and Smith, C.R., Editors, Kluwer Academic, Dordrecht, Germany, 1998, pp. 121-135.

15. Hemez, F.M., and Farhat, C., "Structural Damage Detection Via a Finite Element Model Updating Methodology," *SEM International Journal of Analytical and Experimental Modal Analysis*, Vol. 10, No. 3, July 1995, pp. 152-166.

16. Chouaki, A.T., Ladevèze, P., and Proslier, L., "Updating Structural Dynamics Models With Emphasis on the Damping Properties," *AIAA Journal*, Vol. 36, No. 6, June 1998, pp. 1094-1099.

17. Jacobs, D.A.H., **The State of the Art in Numerical Analysis**, Ed., Academic Press, London, U.K., 1977.

18. Lenaerts, V., Kerschen, G., and Golinval, J.-C., "Parameter Identification of Nonlinear Mechanical Systems Using Proper Orthogonal Decomposition," *18th SEM International Modal Analysis Conference*, San Antonio, Texas, Feb. 7-10, 2000, pp. 133-139.

19. Mees, A.I., Rapp, P.E., and Jennings, L.S., "Singular Value Decomposition and Embedding Dimension," *Physical Review A*, Vol. 36, No. 1, July 1987, pp. 340-346.

20. Mook, D.J, "Estimation and Identification of Nonlinear Dynamic Systems," *AIAA Journal*, Vol. 27, No. 7, July 1989, pp. 968-974.

21. Hemez, F.M., and Doebling, S.W., "Inversion of Structural Dynamics Simulations: State-of-the-art and Orientations of the Research," *25th ISMA International Conference on Noise and Vibration Engineering*, Leuven, Belgium, Sept. 13-15, 2000 (to be published).